45th IEEE International Conference on Acoustics, Speech, and Signal Processing (ICASSP) 2020, 4-8 May 2020, Barcelona, Spain

CRAMER-RAO BOUND ON DOA ESTIMATION OF FINITE BANDWIDTH SIGNALS USING A MOVING SENSOR

Aakash Arora, Bhavani Shankar Mysore R, and Björn Ottersten

Interdisciplinary Centre for Security, Reliability and Trust (SnT), University of Luxembourg
{aakash.arora, bhavani.shankar, bjorn.ottersten}@uni.lu

ABSTRACT

In this paper, we provide a framework for the direction of arrival (DOA) estimation using a single moving sensor and evaluate performance bounds on estimation. We introduce a signal model which captures spatio-temporal incoherency in the received signal due to sensor motion in space and finite bandwidth of the signal, hitherto not considered. We show that in such a scenario, the source signal covariance matrix becomes a function of the source DOA, which is usually not the case. Due to this unknown dependency, traditional subspace techniques cannot be applied and conditions on source covariance needs to imposed to ensure identifiability. This motivates us to investigate the performance bounds through the Cramer-Rao Lower Bounds (CRLBs) to set benchmark performance for future estimators. This paper exploits the signal model to derive an appropriate CRLB, which is shown to be better than those in relevant literature.

Index Terms— DOA estimation, moving sensor, incoherence, multiplicative noise, sub-diagonal sums

1. INTRODUCTION

DOA estimation using a single moving sensor is an interesting problem because of its applicability in diverse areas including speaker and underwater localization as well as interference localization using satellite drifts [1–7]. As a special case, satellite systems are interfered by unintentional/ malicious transmissions requiring rather precise localization on-board; the satellite drift offers a virtual array to solve this issue [7]. Further, the proliferation of sensing capabilities in a variety of devices (i.e. Internet of Things- IoT components) or platforms (i.e. automotive) motivates a revisit to this already well-established topic.

The works [1], [2], focused on DOA estimation with time varying sensor arrays, such as array mounted on a moving platform. In these arrangements, the received signal is assumed to be perfectly coherent throughout the sensor array. When the bandwidth of the source signal is quite large, such as in satellite (few MHz to GHz) [7], coherency across the array cannot be assumed. Further, such loss in coherency is a function of DOA and the signal bandwidth. Another line of work focused on the signal propagation in a random in-homogeneous medium [8, 9]. These works consider a multiplicative noise model to account for wavefront distortion across the array when dealing with a single source. However their model considers a static array; thus the nuances induced by the moving sensor (DOA dependent coherency loss) are not captured. Further, the extension to multiple sources [10], imposes certain structure on the nature of perturbations to ensure identifiability. However, this structure is not considered in evaluating the Cramer-Rao Lower Bound (CRLB). In addition to these aspects, many applications like interference detection on a moving satellite or low complexity solutions using IoT devices at high frequencies involve only one sensor in motion; one then needs to form a virtual array through spatio-temporal sampling.

In this paper, we consider the practically relevant problem of estimating DOA of finite bandwidth signals using a single moving sensor. In this framework, the wavefront amplitude sampled at two different time instants need not be the same. In this context, relevant works include [8, 9] and their findings can be used as a basis to model the loss in coherency for single source scenarios. However, as mentioned earlier, their model does not assume a moving array where the loss in coherency is primarily due to finite bandwidth of the signal (correlated source) rather than an independent multiplicative noise. Further, this multiplicative noise is assumed to be independent of the source DOA, which is restrictive for practical applications [8]. Specifically, for the case of moving sensor where the signal sampled at two-time instants are different, additionally, the effect is more pronounced if there are random fluctuations from the environment. Thus, the existing models do not provide adequate approximations for considered application. Thus, despite the rich literature in DOA, there seems to be an interesting research gap and the current work aims to address.

Our contributions include an appropriate signal model taking into account the direction dependent incoherency in the received signal due to sensor movement, and evaluation of the theoretical performance through CRLB evaluation. The latter helps to evaluate the opportunities and limitations of the framework. To ensure identifiability, the source covariance is modelled as an auto-regressive AR(1) process with real correlation [10] to simulate the finite bandwidth. Exploiting this, the CRLB is derived for the signal model developed and is seen to be different from that in [11], [10]. This difference arises from the exploitation of the model; as a consequence, the benchmark performance can be further improved compared to these works.

2. SYSTEM MODEL

2.1. Scenario and Signal model

Consider a sensor moving with velocity v, receiving signals from P sources in the far-field, $\{x_i(t)\}_{i=1}^{P}$, at M time instants. Let $\mathcal{K} = \{1, 2, \ldots, N\}$, denote the set indicating time indices. The sensor output at time instant t_i is,

$$\tilde{y}(t_i, \boldsymbol{\theta}) = \sum_{k=1}^{P} x_k(t_i - \tau_i(\boldsymbol{\theta}_k)) e^{j2\pi f(t_i - \tau_i(\boldsymbol{\theta}_k))} + \tilde{n}(t_i), i \in \mathcal{K},$$

This work is supported by the National Research Fund (FNR), Luxembourg under the AFR-PPP grant for Ph.D. project SPASAT (Ref.: 11607283), and the CORE-PPP project PROSAT.

where f is the centre frequency of source signal, $x_k(t)$ represents the amplitude of k-th signal arriving from the direction $\boldsymbol{\theta}_k$. Here, $\boldsymbol{\theta}_k \in \mathbb{R}^3$ is the DOA of k-th signal, the vector $\boldsymbol{\theta} = [\boldsymbol{\theta}_1^T, \boldsymbol{\theta}_2^T, \ldots, \boldsymbol{\theta}_P^T]^T$ consists of P source DOAs. Further, $\tau_i(\boldsymbol{\theta}_k)$ is time required by the kth signal to arrive at the sensor and depends on the direction of propagation and sensor position. Furthermore, $\tilde{n}(t_i) \in \mathcal{CN}(0, \sigma), \forall i \in \mathcal{K}$, is temporally i.i.d. complex zero-mean Gaussian noise samples with variance σ. The sensor output after demodulation is,

$$y(t_i, \boldsymbol{\theta}) = \sum_{k=1}^{P} x_k(t_i - \tau_i(\boldsymbol{\theta}_k)) e^{-j2\pi f \tau_i} + n(t_i). \tag{1}$$

Collecting N measurements, $[\mathbf{y}(\boldsymbol{\theta})]_i = y(t_i, \boldsymbol{\theta})$, and writing them in compact form yields,

$$\mathbf{y}(\boldsymbol{\theta}) = \sum_{k=1}^{P} \mathbf{x}_k(\boldsymbol{\theta}_k) \circ \mathbf{a}(\theta_k) + \mathbf{n}, \tag{2}$$

where $[\mathbf{x}_k(\boldsymbol{\theta}_k)]_i = x(t_i - \tau_i(\boldsymbol{\theta}_k))$, $[\mathbf{a}(\boldsymbol{\theta}_k)]_i = e^{-j2\pi f \tau_i(\boldsymbol{\theta}_k)}$, and $[\mathbf{n}]_i = n(t_i)$. The symbol $\circ$ denotes element-wise product between the two vectors/matrices. The covariance matrix of the measurement vector $\mathbf{y}(\boldsymbol{\theta})$ can be readily written as,

$$\mathbf{R}(\boldsymbol{\theta}) = \sum_{k=1}^{P} \mathbf{R}_{x_k}(\boldsymbol{\theta}_k) \circ \mathbf{a}(\boldsymbol{\theta}_k)\mathbf{a}^H(\boldsymbol{\theta}_k) + \sigma \mathbf{I}, \tag{3}$$

where $\mathbf{R}_{x_k}(\boldsymbol{\theta}_k) = \mathbb{E}\{[\mathbf{x_k}(\boldsymbol{\theta_k})][\mathbf{x_k}(\boldsymbol{\theta_k})]^H\}$ is the source covariance matrix evaluated at certain lags (given by t_i, τ_i). Details on obtaining sampled covariance matrix is presented in Section 3.

While (3) is valid for any sampling and direction of motion, we assume a linear sensor motion. We further assume that the sensor samples the wavefront uniformly at distances $d = \frac{\lambda}{2}$, where $\lambda = \frac{c}{f}$, and c is the signal propagation speed. The sampling instances are then given by $t_i = t_1 + (i-1)\frac{d}{v}$. Let $\delta = t_{i+1} - t_i = \frac{d}{v}, \forall i$. The phase difference for the k-th signal received at i-th time instant with respect to the first sampling instant can be written as $\tau_i(\boldsymbol{\theta}_k) - \tau_1(\boldsymbol{\theta}_k) = (i-1)\frac{d \sin\theta_k}{c}$. We further assume that $(M-1)\frac{d \sin\theta_k}{c} << \delta$.

2.1.1. Spatio-Temporal Incoherency

The received covariance in (3) has a form similar to the works considering waveform distortion across a static array [8, 9]. However, it can be inferred from (3) that $\mathbf{R}_{x_k}$ depends on the source DOA, which is not the case in the aforementioned works. The exact form of $\mathbf{R}_{x_k}$ depends the source modelling. The dependence of the amplitude of $x_k(t)$ on $\boldsymbol{\theta}_k$ differentiates the proposed model from DOA independent perturbation in [12], [10]. This results in DOA dependent perturbations associated with each source; this effect has been mentioned but not investigated in literature e.g. [8].

2.2. Covariance Model

Similar to [10], we consider the kth source to be a zero-mean circularly symmetric Gaussian AR(1) process, $x_k(t_i) = \alpha_k x_k(t_{i-1}) + n_k(t_i)$, where $-1 < \alpha_k < 1$ and $\{n_k(t_i)\} \in \mathcal{N}(0, \sigma_{s_k})$ are samples of a temporally and spatially independent Gaussian noise with variance, $\{\sigma_{s_k}\}$. The condition $|\alpha_k| < 1$, ensures stability of the process. Using the sampling assumptions in Section 2.1 including $(M-1)\frac{d \sin\theta_k}{c} << \delta$ and the AR(1) model for sources, it follows that, $\mathbf{R}_{x_k}(\boldsymbol{\theta}_k)$ is a Hermitian Toeplitz matrix whose first row is, $\beta_k \left[1, \alpha_k^{\delta + \frac{d \sin\theta_k}{c}}, \ldots, \alpha_k^{(M-1)\left(\delta + \frac{d \sin\theta_k}{c}\right)}\right]$, where $\beta_k = \frac{\sigma_{s_k}}{1-\alpha_k^2}$, is the variance of $x_k(t)$. When $\alpha_k \in (-1, 0)$ and $\Delta \in \mathbb{R}$, then α_k^{Δ} can be complex, resulting in phase ambiguity. Thus, we constrain $\alpha_k \in (0, 1), \forall k$ so that each entry of $\mathbf{R}_{x_k}(\boldsymbol{\theta}_k)$ is a real number.

Since the source signals have a real correlation, it can be shown that the real and imaginary parts of the source signal are independent of each other and identically distributed. Hence, it can be shown that $\mathbb{E}\{[\mathbf{x_k^R}(\boldsymbol{\theta_k})][\mathbf{x_k^R}(\boldsymbol{\theta_k})]^T\} = \mathbb{E}\{[\mathbf{x_k^I}(\boldsymbol{\theta_k})][\mathbf{x_k^I}(\boldsymbol{\theta_k})]^T\} = \frac{1}{2}\mathbf{R}_{x_k}(\boldsymbol{\theta}_k)$, where, $\mathbf{x}_k^R(\boldsymbol{\theta}) = \mathrm{Re}\{\mathbf{x}_k(\boldsymbol{\theta})\}$ and $\mathbf{x}_k^I(\boldsymbol{\theta}) = \mathrm{im}\{\mathbf{x}_k(\boldsymbol{\theta})\}$. To exploit this fact, we obtain the covariance matrix of $\tilde{\mathbf{y}}(\boldsymbol{\theta}) = [\mathbf{y}_R^T(\boldsymbol{\theta}), \mathbf{y}_I^T(\boldsymbol{\theta})]^T \in \mathbb{R}^{2M \times 1}, \mathbf{y}_R(\boldsymbol{\theta}) = \mathrm{Re}\{\mathbf{y}(\boldsymbol{\theta})\}$ and $\mathbf{y}_I(\boldsymbol{\theta}) = \mathrm{im}\{\mathbf{y}(\boldsymbol{\theta})\}$. Towards this, we first let $\tilde{\mathbf{a}}_k(\boldsymbol{\theta}_k) = [\mathbf{a}_R^T(\boldsymbol{\theta}_k), \mathbf{a}_I^T(\boldsymbol{\theta}_k)]^T \in \mathbb{R}^{2N \times 1}, \mathbf{a}_R(\boldsymbol{\theta}_k) = \mathrm{Re}\{\mathbf{a}(\boldsymbol{\theta}_k)\}$ and $\mathbf{a}_I(\boldsymbol{\theta}_k) = \mathrm{im}\{\mathbf{a}(\boldsymbol{\theta}_k)\}$. The covariance matrix of the vector $\tilde{\mathbf{y}}$ after some manipulations takes the form,

$$\tilde{\mathbf{R}} = \frac{1}{2}\sum_{k=1}^{P} \tilde{\mathbf{A}}_k \left(\mathbf{I}_2 \otimes \mathbf{R}_{x_k}\right) \tilde{\mathbf{A}}_k^T + \frac{\sigma}{2}\mathbf{I}, \tag{4}$$

where $\tilde{\mathbf{A}}_k = \begin{bmatrix} \mathrm{diag}\left(\mathbf{a}_R(\boldsymbol{\theta}_k)\right) & -\mathrm{diag}\left(\mathbf{a}_I(\boldsymbol{\theta}_k)\right) \\ \mathrm{diag}\left(\mathbf{a}_I(\boldsymbol{\theta}_k)\right) & \mathrm{diag}\left(\mathbf{a}_R(\boldsymbol{\theta}_k)\right) \end{bmatrix}$, $\mathbf{I}_2$ is a 2×2 identity matrix and $\otimes$ is the Kronecker product. The model in (4) differs from the earlier works, both in the dependence of $\mathbf{R}_{x_k}$ on DOA as well as the exploitation of the source modeling; these have not been considered hitherto. The rank of each $(\mathbf{R}_{x_k}(\boldsymbol{\theta}_k)) = N$ and hence the signal subspace dimension can be greater than P [13]. This results in ambiguity in detection even in the absence of noise, and one cannot estimate the number and DOA of sources using conventional subspace methods [14], [15]. Towards formulating the DOA estimation algorithms, we now focus on understanding the benchmark performance through the derivation of CRLB.

3. CRLB DERIVATION

Under the assumptions on the transmitted signals, the measurement vector $\tilde{\mathbf{y}}(\boldsymbol{\theta}) \in \mathcal{N}(\mathbf{0}, \tilde{\mathbf{R}}(\boldsymbol{\theta}, \boldsymbol{\alpha}, \boldsymbol{\sigma}_s, \sigma))$ where $\mathbf{0}$ denotes the N dimensional zero vector, $\boldsymbol{\alpha} = [\alpha_1, \alpha_2, \ldots, \alpha_P]^T$, and $\boldsymbol{\sigma}_s = [\sigma_{s_1}, \sigma_{s_2}, \ldots, \sigma_{s_P}]^T$. Therefore, the CRLB for the unknown parameters can be computed by inverting the Fisher information matrix [16], [17], whose entries can be written as,

$$\mathbf{F}(k, l) = N \,\mathrm{Tr}\left\{\mathbf{R}^{-1}\frac{\partial \mathbf{R}}{\partial \boldsymbol{\eta}_k}\mathbf{R}^{-1}\frac{\partial \mathbf{R}}{\partial \boldsymbol{\eta}_l}\right\}, \tag{5}$$

where $\boldsymbol{\eta} = [\boldsymbol{\theta}, \boldsymbol{\alpha}, \boldsymbol{\sigma}_s, \sigma]^T \in \mathbb{R}^{5P+1}$, is the true parameter vector, N are the number of independent measurements available.

For ease of presentation, we omit the dependence of $\mathbf{R}$ and $\mathbf{R}_x$ on $\boldsymbol{\theta}, \boldsymbol{\alpha}, \boldsymbol{\sigma_s}$ and use $\mathbf{a}_k = \mathbf{a}(\boldsymbol{\theta}_k)$. In this context, the key derivatives are presented in Table 1 at the top of the next page. In that table, $Toeplitz\left(\{q_i\}_{i=1}^{M}\right)$ is a Symmetric Toeplitz matrix with the first row formed using the elements $\{q_i\}$. Further, the elements of $\frac{\partial \tilde{\mathbf{A}}}{\partial \theta_k}$ can be found by differentiating $\cos\frac{(m-1)d\sin\theta_k}{c}$ and $\sin\frac{(m-1)d\sin\theta_k}{c}$ appropriately. .

Evaluating the CRLB expression in closed-form is a difficult task in general a special case is considered below.

Theorem 1. *For the special case of single source, the elements of*

Table 1: Derivatives used in the CRLB derivation

$\tilde{\mathbf{R}}'_{\theta_k} \triangleq \frac{\partial \tilde{\mathbf{R}}}{\partial \theta_k}$	$\frac{\partial \tilde{\mathbf{A}}_k}{\partial \theta_k}\mathbf{R}_{x_k}\tilde{\mathbf{A}}_k^T + \tilde{\mathbf{A}}_k\mathbf{R}_{x_k}\frac{\partial \tilde{\mathbf{A}}_k^T}{\partial \theta_k} + \tilde{\mathbf{A}}_k\mathbf{R}'_{x_k,\theta_k}\tilde{\mathbf{A}}_k^T$
$\mathbf{R}'_{x_k,\theta_k} \triangleq \frac{\partial \mathbf{R}_{x_k}}{\partial \theta_k}$	$Toeplitz\left(\left\{\frac{-d(m-1)}{c}\ \ln(\alpha_k)\ \cos\theta_k\ \alpha_k^{(m-1)(\delta-\frac{d\sin\theta_k}{c})}\right\}_{m=1}^{M}\right)$
$\mathbf{R}'_{x_k,\alpha_k} \triangleq \frac{\partial \tilde{\mathbf{R}}}{\partial \alpha_k}$	$Toeplitz\left(\left\{\left[\delta(m-1)\frac{d\sin\theta_k}{c}\right]\ \alpha_k^{(m-1)(\delta-\frac{d\sin\theta_k}{c})}\right\}_{m=1}^{M}\right) + \frac{-2\alpha_k}{(1-\alpha_k^2)^2}\mathbf{R}_{x_k}$
$\tilde{\mathbf{R}}'_{x_k,\sigma} \triangleq \frac{\partial \tilde{\mathbf{R}}}{\partial \sigma}$	$\mathbf{I}_{2M}$
$\tilde{\mathbf{R}}'_{x_k,\sigma_{s_k}} \triangleq \frac{\partial \tilde{\mathbf{R}}}{\partial \sigma_{s_k}}$	$\frac{1}{\sigma_{s_k}}\tilde{\mathbf{A}}_k\mathbf{R}_{x_k}\tilde{\mathbf{A}}_k^T$

the Fischer information matrix can be evaluated as:

$$\begin{aligned}
\mathbf{F}(1,1) &= 4\,\mathrm{Tr}\left\{\mathbf{X}^{-1}\mathbf{\Lambda}\mathbf{X}\mathbf{\Lambda}\right\} - 4\,\mathrm{Tr}\left\{\mathbf{\Lambda}^2\right\} \\
&+ 4\,\mathrm{Tr}\left\{\mathbf{X}^{-1}\mathbf{R}'_{x_1,\theta_1}\mathbf{X}^{-1}\mathbf{R}'_{x_1,\theta_1}\right\} \quad (6)\\
\mathbf{F}(1,2) &= 2\,\mathrm{Tr}\left\{\mathbf{X}^{-1}\mathbf{R}'_{x_1,\theta_1}\mathbf{X}^{-1}\mathbf{R}'_{x_1,\alpha_1}\right\} \quad (7)\\
\mathbf{F}(1,3) &= 2\,\mathrm{Tr}\left\{\mathbf{X}^{-1}\mathbf{R}'_{x_1,\theta_1}\mathbf{X}^{-1}\mathbf{R}'_{x_1,\sigma_{s_1}}\right\} \quad (8)\\
\mathbf{F}(1,4) &= \mathrm{Tr}\left\{\mathbf{X}^{-1}\mathbf{R}'_{x_1,\theta_1}\mathbf{X}^{-1}\right\} \quad (9)\\
\mathbf{F}(2,2) &= 2\,\mathrm{Tr}\left\{\mathbf{X}^{-1}\mathbf{R}'_{x_1,\alpha_1}\mathbf{X}^{-1}\mathbf{R}'_{x_1,\alpha_1}\right\}\\
\mathbf{F}(2,3) &= 2\,\mathrm{Tr}\left\{\mathbf{X}^{-1}\mathbf{R}'_{x_1,\alpha_1}\mathbf{X}^{-1}\mathbf{R}'_{x_1,\sigma_{s_1}}\right\}\\
\mathbf{F}(2,4) &= \mathrm{Tr}\left\{\mathbf{X}^{-1}\mathbf{R}'_{x_1,\alpha_1}\mathbf{X}^{-1}\right\}\\
\mathbf{F}(3,3) &= 2\,\mathrm{Tr}\left\{\mathbf{X}^{-1}\mathbf{R}'_{x_1,\sigma_{s_1}}\mathbf{X}^{-1}\mathbf{R}'_{x_1,\sigma_{s_1}}\right\}\\
\mathbf{F}(3,4) &= 2\,\mathrm{Tr}\left\{\mathbf{X}^{-1}\mathbf{R}'_{x_1,\sigma_{s_1}}\mathbf{X}^{-1}\right\}\\
\mathbf{F}(4,4) &= \frac{1}{2}\,\mathrm{Tr}\left\{\mathbf{X}^{-1}\mathbf{X}^{-1}\right\}
\end{aligned}$$

where $\mathbf{X} = \mathbf{R}_{x_1} + \frac{\sigma}{2}\mathbf{I}$ *and* $\mathbf{\Lambda}$ *is a* $M \times M$ *matrix which is extracted from* $\tilde{\mathbf{A}}_1^T\frac{\partial \tilde{\mathbf{A}}_1}{\partial \theta_1}$ *as* $\tilde{\mathbf{A}}_1^T\frac{\partial \tilde{\mathbf{A}}_1}{\partial \theta_1} = \begin{bmatrix} \mathbf{0} & \mathbf{\Lambda} \\ -\mathbf{\Lambda} & \mathbf{0} \end{bmatrix}$

Proof: The derivation follows from standard matrix manipulations after noting the structure of various matrices and their derivatives given in Table 1; the details are omitted for brevity.

In the following remarks, some insights drawn from analysing the aforementioned expressions will be provided. The focus will be on the performance of DOA estimation in this work.

Remark 1. *Dependence on DOA:* It should be noted that $\mathbf{R}'_{x_1,\theta_1}$ appears in the CRLB; this term is unique to the model considered in this paper and arises from the dependence of $\mathbf{R}_{x_1,\theta_1}$ on DOA. This term introduces dependence of estimating θ on the other parameters. This impact can be gauged from the fact that $\mathbf{F}(1,2) = \mathbf{F}(1,3) = \mathbf{F}(1,4) = 0$ when $\mathbf{R}'_{x_1,\theta_1} = 0$.

Remark 2. *CRLB performance with SNR:* When $\mathbf{R}_{x_1,\theta_1}$ is negligible (ideally zero), CRLB of θ_1 is independent of the other estimation variables. Further, $\mathbf{F}(1,1)$ exists even in the absence of the noise term as $\mathbf{R}$ is full rank. Under such conditions, CRLB of θ_1 approaches a finite value away from zero asymptotically in SNR.

Remark 3. *CRLB performance with* α_1*:* It is difficult to establish an elegant closed-form relation between α_1 and CRLB of θ_1. It can however, be argued that, as α increases, the source tends to become narrow band and the CRLB improves.

Multiple sources: Simplification of CRLB of θ is cumbersome in this case. However, as in many studies, the CRLB also depends on the difference between the different θ_k's.

Now, we numerically evaluate the CRLB for various SNR under different choices of the source parameters. We note that the sensor has N samples of the wavefront corresponding to the scenario under test. We now begin with the simulation set-up.

4. NUMERICAL EVALUATION

We consider a sensor linearly moving with $v = 3$km/s and sampling a far-field signal. Both single and dual source scenarios are considered with $f = 30$GHz which corresponds to a typical satellite operation. Unless mentioned otherwise $M = 10$ is chosen and $N = 1000$ samples chosen. The SNR (in dB) is calculated using the relation $10\log_{10}\left(\frac{\beta}{\sigma}\right)$ and $\sigma = 1$. The RMSE in DOA estimates refers to the CRLB of θ.

As a benchmark, the CRLB derived in [10] is appropriately used. That work does not consider the simplification of the CRLB due to the exploitation of the real AR(1) parameters (in the noise model of [10]). This is denoted as *benchmark* in the results.

Performance of Single Source versus SNR

Fig. 1 depicts the performance of a single source for different source parameters. It should be noted that a smaller α refers to a wide band source. Clearly, the CRLB degrades when the α reduces to zero. As mentioned in previous works, it also floors to a non-zero value. Further, we also note that a better performance can be targetted when exploiting the source model.

Performance of Two Sources versus SNR

Fig. 2 depicts the performance of two sources $(10^o, 2^o)$ for different source parameters; the sum RMSE for the two angles is considered. The influence of one source distribution on the other is clearly seen. Further, when α_2 is increased keeping α_1 fixed, like in the single source case, the CRLB improves. Finally, we also note that a better performance can be targetted when exploiting the source model.

Further Fig. 3 shows the variation in the sum of CRLB(θ_1) and CRLB(θ_2) for different source separations. This shows that the CRLB depends on the angular separation of the sources, a matter that needs further investigation.

Performance with fixed number of time samples

Fig. 4 depicts the relative CRLB for a single source when the sensor aims to utilize $N = 10000$ samples as N/M independent realizations of the wavefront on M sensors. It should be noted that the

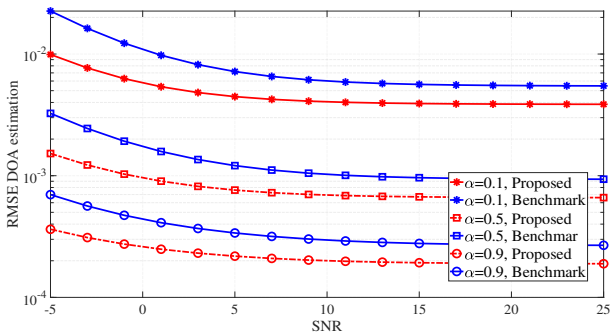

Fig. 1: Variation of RMSE (in radians) of a single source at 10^o as a function of AR parameter; proposed and benchmark values included with SNR measured in dB.

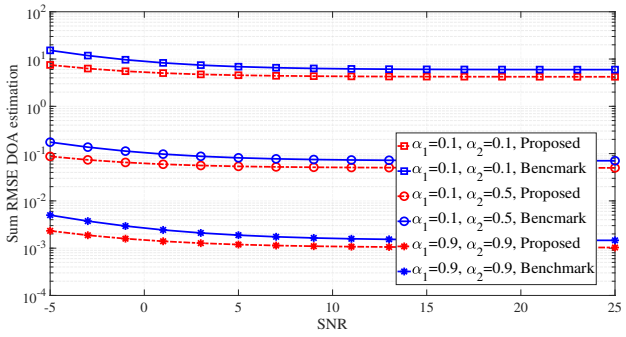

Fig. 2: Variation of RMSE (in radians) of two sources at $10^o, 2^o$ as a function of AR parameters; proposed and benchmark values included. SNR measured in dB

bound need not be attained since the samples are correlated (AR(1) modelling), while they are assumed independent. This bound gives an insight to practical set-ups where a case where the sensor has a fixed number of samples and then splits it into blocks of M samples, with each block corresponding to an array. While it is better to use a large M, the lack of available samples make it difficult to estimate statistics; the complexity tends to be higher as well. On the other hand, lower number of arrays, naturally limit the performance. These aspects are captured in Fig. 4, where, the performance improves with the number of sensors first (due to increased aperture) followed by a degradation (due to lower number of samples). In Fig. 4, the relative loss in CRLB with regards to $M = 25$ sensors is considered; both the proposed and benchmark techniques provide similar result and only one is depicted.

Performance with varying number of time samples

The scenario considered here is similar to one considered earlier, however, with M fixed to 10 and N is varied. Fig. 5 depicts the CRLB of θ_1 and it follows the trend of gradual decay.

5. CONCLUSION

This paper considered the problem of estimating the finite bandwidth source DOA using single moving sensor. A key motivation is the proliferation of sensing capabilities in cheap IoT devices as well as novel applications including satellite communication. The derived signal model was presented and takes into account the spatio-

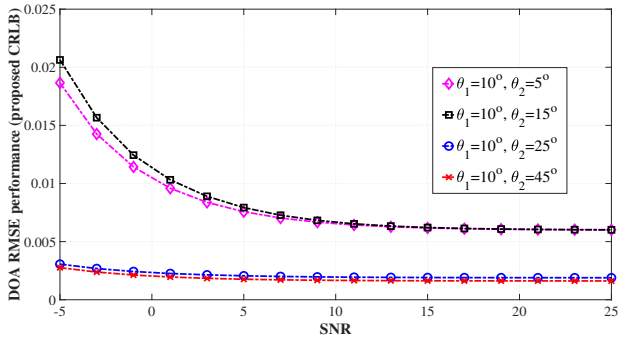

Fig. 3: Dependence of RMSE (in radians) on angular location of two sources, fixed AR parameters; proposed CRLB expression only. SNR measured in dB

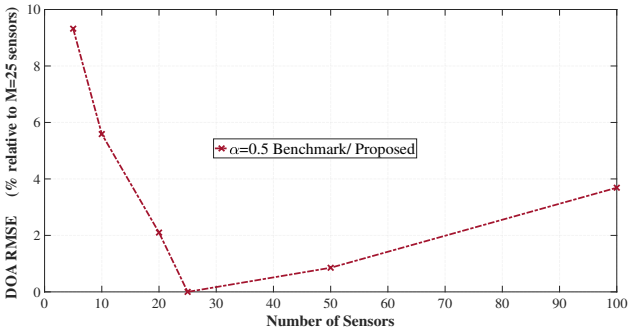

Fig. 4: Variation of relative RMSE as a function of number of sensors with maximum number of measurements fixed to 10000, single source, DOA=10^o, SNR=10dB and $\alpha = 0.5$.

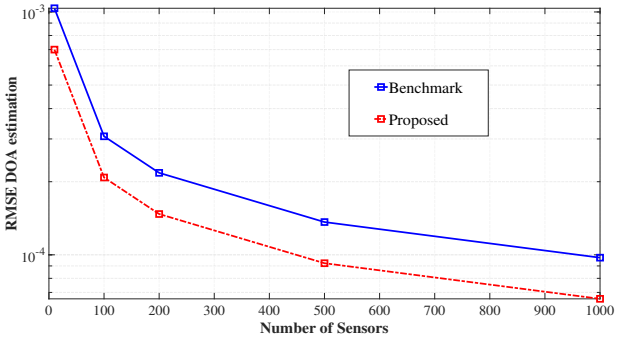

Fig. 5: Variation of RMSE (in radians) as a function of number of measurements, $M = 10$, single source, DOA=10^o, SNR=10dB.

temporal incoherency in the wavefront sampled by the sensor at distinct time instants due to non-zero bandwidth of the signals. This model generalizes the existing work on incoherency. Based on identifiability, certain structure is imposed on the source covariance and is exploited by the current work to further refine the CRLB available in literature. Using the derived CRLB, numerical evaluations are resorted to understand the influence of various system parameters on performance and provide system designers information about the system limitations. An analytical treatment and derivation of estimators is left for future work.

6. REFERENCES

[1] J. Sheinvald, M. Wax, and A. J. Meiss, "Localization of multiple sources with moving arrays," *IEEE Trans. Signal Process.*, vol. 46, no. 10, pp. 2736–2743, Oct 1998.

[2] F. Haber and M. Zoltowski, "Spatial spectrum estimation in a coherent signal environment using an array in motion," *IEEE Trans. Antennas Propag.*, vol. 34, no. 3, pp. 301–310, March 1986.

[3] A. B. Gershman, V. I. Turchin, and V. A. Zverev, "Experimental results of localization of moving underwater signal by adaptive beamforming," *IEEE Trans. Signal Process.*, vol. 43, no. 10, pp. 2249–2257, Oct 1995.

[4] E. Y. Gorodetskaya, A. I. Malekhanov, A. G. Sazontov, and N. K. Vdovicheva, "Deep-water acoustic coherence at long ranges: theoretical prediction and effects on large-array signal processing," *IEEE J. Ocean. Eng.*, vol. 24, no. 2, pp. 156–171, April 1999.

[5] M. Omologo and P. Svaizer, "Acoustic event localization using a crosspower-spectrum phase based technique," in *Proceedings of ICASSP '94. IEEE International Conference on Acoustics, Speech and Signal Processing*, April 1994, vol. ii, pp. II/273–II/276 vol.2.

[6] Michael S. Brandstein and Harvey F. Silverman, "A practical methodology for speech source localization with microphone arrays," *Computer Speech & Language*, vol. 11, no. 2, pp. 91 – 126, 1997.

[7] A. Arora, S. Maleki, B. S. M. Rama Rao, J. Grotz, and B. Ottersten, "Interference localization on-board the satellite using drift induced virtual array," in *2018 International Conference on Signal Processing and Communications (SPCOM)*, July 2018, pp. 467–471.

[8] J. Ringelstein, A. B. Gershman, and J. F. Bohme, "Direction finding in random inhomogeneous media in the presence of multiplicative noise," *IEEE Signal Process. Lett.*, vol. 7, no. 10, pp. 269–272, Oct 2000.

[9] P. Stoica, O. Besson, and A. B. Gershman, "Direction-of-arrival estimation of an amplitude-distorted wavefront," *IEEE Trans. Signal Process.*, vol. 49, no. 2, pp. 269–276, Feb 2001.

[10] M. Ghogho, O. Besson, and A. Swami, "Estimation of directions of arrival of multiple scattered sources," *IEEE Trans. Signal Process.*, vol. 49, no. 11, pp. 2467–2480, Nov 2001.

[11] O. Besson, F. Vincent, P. Stoica, and A. B. Gershman, "Approximate maximum likelihood estimators for array processing in multiplicative noise environments," *IEEE Trans. Signal Process.*, vol. 48, no. 9, pp. 2506–2518, Sep. 2000.

[12] O. Besson, P. Stoica, and A. B. Gershman, "Simple and accurate direction of arrival estimator in the case of imperfect spatial coherence," *IEEE Trans. Signal Process.*, vol. 49, no. 4, pp. 730–737, April 2001.

[13] M. Bengtsson and B. Ottersten, "A generalization of weighted subspace fitting to full-rank models," *IEEE Trans. Signal Process.*, vol. 49, no. 5, pp. 1002–1012, May 2001.

[14] M. Viberg and B. Ottersten, "Sensor array processing based on subspace fitting," *IEEE Trans. Signal Process.*, vol. 39, no. 5, pp. 1110–1121, May 1991.

[15] P. Stoica and A. Nehorai, "MUSIC, maximum likelihood, and Cramer-Rao bound," *IEEE Trans. Acoust., Speech, Signal Process.*, vol. 37, no. 5, pp. 720–741, May 1989.

[16] P. Stoica, E. G. Larsson, and A. B. Gershman, "The stochastic CRB for array processing: a textbook derivation," *IEEE Signal Process. Lett.*, vol. 8, no. 5, pp. 148–150, May 2001.

[17] Petre Stoica and Randolph L. Moses, *Spectral Analysis of Signals*, Prentice Hall, Upper Saddle River, NJ, 2005.